Science of the Total Environment 790 (2021) 148147

Contents lists available at ScienceDirect

Science of the Total Environment

journal homepage: www.elsevier.com/locate/scitotenv

Modeling salinity drop in estuarine areas under extreme precipitation events within a context of climate change: Effect on bivalve mortality in Galician Rías Baixas

M. Des [a,*], D. Fernández-Nóvoa [a], M. deCastro [a], J.L. Gómez-Gesteira [a], M.C. Sousa [b], M. Gómez-Gesteira [a]

[a] Centro de Investigación Mariña, Universidade de Vigo, Environmental Physics Laboratory (EPhysLab), Campus As Lagoas s/n, Ourense 32004, Spain
[b] CESAM, Physics Department, University of Aveiro, Aveiro 3810-193, Portugal

HIGHLIGHTS

- Climate change impacts on extreme precipitations and river runoff.
- Increase of extreme river discharges may lead to higher salinity drops in estuarine areas.
- Effect of salinity drops on the mortality of bivalves near river mouths.
- Bivalves' mortality increases when extreme river runoff and neap tides match.
- The physiography of the estuary is crucial to determine the death rate.

GRAPHICAL ABSTRACT

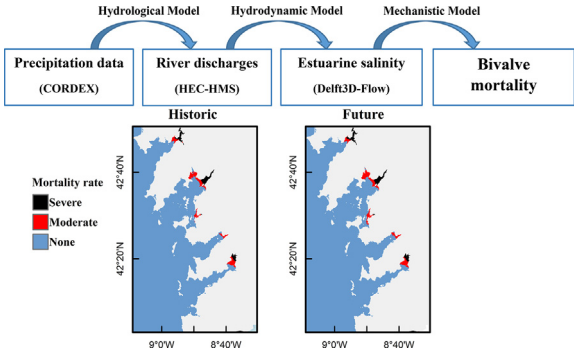

ARTICLE INFO

Article history:
Received 8 February 2021
Received in revised form 18 May 2021
Accepted 25 May 2021
Available online 29 May 2021

Editor: Christian Herrera

Keywords:
Bivalve mortality
Climate change
Ecological modeling
Extreme precipitation events
Hydrodynamic modeling
Hydrologic modeling

ABSTRACT

The mortality of infaunal bivalves (*Venerupis corrugata*, *Cerastoderma edule*, *Ruditapes decussatus* and *Ruditapes philippinarum*) due to a drop in salinity caused by extreme precipitation events in estuarine areas has been analyzed within a context of climate change. The Rías Baixas (NW Iberian Peninsula) were selected as a representative area of the estuarine environments where bivalve gathering is performed. Bivalve mortality under extreme precipitation events was analyzed both for historical (1990–2019) and future (2070–2099) periods. Precipitation data were retrieved from the Coordinated Regional Climate Downscaling Experiment (CORDEX) project under the Representative Concentration Pathway (RCP) 8.5 scenario and were converted into river discharges using the HEC-HMS hydrological model. The calculated river discharges were introduced into the Delft3D hydrodynamic model and simulations were performed in order to calculate transport conditions in the Rías Baixas. Salinity data were analyzed to estimate the mortality of the species due to salinity drops. In general, future conditions of moderate and severe mortality may be worse than historically observed, being more intense and covering larger areas. This is mainly observed under neap tides due to less dilution of freshwater plumes when compared with spring tides. Although all the Rías Baixas may be potentially affected, the impact will differ for each ria, being Arousa, where the highest discharges occur, the most affected. The differences among rias, especially those with a similar discharge pattern as Pontevedra and Vigo, suggest that bathymetric features also play a key role in the extent of the area affected by mortality.
© 2021 The Authors. Published by Elsevier B.V. This is an open access article under the CC BY-NC-ND license (http://creativecommons.org/licenses/by-nc-nd/4.0/).

* Corresponding author.
E-mail address: mdes@uvigo.es (M. Des).

https://doi.org/10.1016/j.scitotenv.2021.148147
0048-9697/© 2021 The Authors. Published by Elsevier B.V. This is an open access article under the CC BY-NC-ND license (http://creativecommons.org/licenses/by-nc-nd/4.0/).

1. Introduction

There is evidence that extreme precipitation events in extratropics may become more intense and frequent due to climate change (Algarra et al., 2020; Fischer and Knutti, 2016; Kharin et al., 2013; Myhre et al., 2019; Stocker et al., 2014). The interest in studying and understanding extreme precipitation events has grown worldwide because they may generate landslides, floods, and disturb social and economic activities (Hosseinzadehtalaei et al., 2020; Kunkel et al., 1999; Mukherjee et al., 2018; Vázquez et al., 2020). During these events the rivers flow increases considerably, leading to the rise in the inflow of fresh water in estuarine areas affecting many species. Estuaries are suitable for aquaculture and, in many of them, it is focused on the cultivation and collection of shellfish, mainly bivalves. Shellfish productivity and survival depend mainly on salinity (Munroe et al., 2013; Parada and Molares, 2008). Sudden salinity drops cause significant effects in bivalves, such as altering feeding, respiration, growth, osmoregulation, behavior, reproduction, and parasite-disease interactions (Gosling, 2008) and, depending on the intensity and duration of the episodes, they can also lead to massive mortality (Gledhill et al., 2020; Peteiro et al., 2018). Thereby, extreme precipitation events can have a significant ecological impact and lead to a tremendous economic cost (Parada et al., 2012; Sobral and Fernandes, 2004; Verdelhos et al., 2015).

Several studies have analyzed the response of bivalves to different ranges of salinity over the time designing laboratory experiments (Berger and Kharazova, 1997; Carregosa et al., 2014; Domínguez et al., 2020; Peteiro et al., 2018; Pourmozaffar et al., 2020; Verdelhos et al., 2015; Woodin et al., 2020). These researches provide very valuable information on the physiological response of different species at different salinity ranges and exposure times, but they face the problem of reproducing natural conditions in the most realistic way possible. Parada et al. (2012) analyzed multiple episodes of mortality of *Venerupis corrugata*, *Cerastoderma edule*, *Ruditapes decussatus* and *Ruditapes philippinarum* related with extreme precipitation events and salinity variations in the inner part of the Ría de Arousa (Rías Baixas). The *in situ* data and the development of numerical models allowed them to determine the relationship between variations in salinity and mortality rates of these species.

The Rías Baixas are located on the northwest coast of the Iberian Peninsula at the northern limit of the Eastern North Atlantic Upwelling system. The rias are high primary productivity areas, home of the principal marine aquaculture industries in Europe (Aguiar et al., 2017; FAO, 2016). One of the most important economic activities is shellfishery, and most of the shellfish banks are located in the inner part of the rias, where the main rivers discharge. In these areas, *V. corrugata*, *C. edule*, *R. decussatus* and *R. philippinarum* are the main gathered species. Data from the regional government (Consellería do Mar, Xunta de Galicia) indicate that more than 7500 tons of these species with a landed value of approximately €71 million were produced during the 2019 in the Rías Baixas (https://www.pescadegalicia.gal, accessed January 2021).

In the Rías Baixas, rivers show a seasonal pattern with the highest discharges during winter months, causing a drop in salinity and subjecting shellfish banks to stress conditions. In many cases, salinity reaches values below the optimal lower limit for many bivalve species, but these events only last for a short period, not having a significant impact on productivity. However, when extreme precipitation events occur, salinity values may remain below the lower tolerance limit for extended periods leading to massive mortalities of shellfish (Parada et al., 2012; Parada and Molares, 2008). Technical reports from the Galician Government show mortality episodes of commercial species associated with extreme precipitation events and, in some cases, they referred to the total or practically total mortality of the bivalves (Parada et al., 2012).

Future projections indicate that extreme precipitation events may be more intense in the Iberian Peninsula during autumn and winter (Cardoso Pereira et al., 2020; de Melo-Gonçalves et al., 2016; Lorenzo and Alvarez, 2020). This intensification implies that the input of freshwater into the Rías Baixas may increase, breaking the balance of salinity and affecting the production of many bivalve species. Despite the fact that this could cause significant economic damage, no studies have been found that analyze the possible effect of extreme precipitation events on bivalve production. Filgueira et al. (2016) have analyzed the response of an ecosystem located in a hypothetic bay with aquaculture activities of *Mytilus edulis* and *Crassostrea virginica*, with similar characteristics to the Gulf of St. Lawrence (GSL, Eastern Canada), to changes in several drivers, among which is precipitation, due to climate change using a hydrodynamic–biogeochemical coupled model. However, they do not analyze extreme precipitation events or the effects of salinity drops caused by precipitation on bivalves.

The present study attempts to determine how intensification in extreme precipitation events due to climate change will affect shellfish aquaculture in estuarine areas under projected conditions. To achieve this goal, the Rías Baixas were chosen as study area because their significant aquaculture activities in shallow areas, focused in the collection of *V. corrugata*, *C. edule*, *R. decussatus* and *R. philippinarum*. First, precipitation data from Regional Climate Models (RCMs) were evaluated in order to obtain the mean precipitation over the wet season and the representative precipitation of 10-year and 50-year return periods precipitation events for the historical (1990–2019) and future (2070–2099). Then, precipitation data was imposed into a hydrological model (HEC-HMS) computing the discharge of the main rivers flowing into the Rías Baixas. These river discharges were imposed into a Hydrodynamic model (Delft3D-Flow) which calculates the salinity conditions on the Rías Baixas under such precipitation events. Finally, salinity data was used to assess the areas where mortality of *V. corrugata*, *C. edule*, *R. decussatus* and *R. philippinarum* may occur.

2. Area of study

The Rías Baixas, located in the NW coast of the Iberian Peninsula, are four flooded incised valleys (Evans and Prego, 2003), which follow a general SW-NE orientation. From north to south they are Muros, Arousa, Pontevedra and Vigo rias (Fig. 1). According to their hydrodynamic and sedimentological characteristics, they are generally divided into three sectors: inner, middle and outer. The inner sector comprises the shallow head of the ria where the mouths of the main rivers are usually located. The middle sector corresponds to the central part of the ria and is characterized by a low-energy regime and the outer sector corresponds the mouth of the ria and connects it to the shelf. In most of cases, there are islands and peninsulas in the outer part that protect the ria from the direct and energetic influence of the ocean (Vilas, 2009). The bathymetry of the rias shows a valley geometry, deeper along the central axes with depths decreasing gradually from the outer sector to the head.

Hydrographically, the Rías Baixas are partially mixed estuaries characterized by a partially stratified estuarine circulation (Taboada et al., 1998). The typical residual circulation pattern corresponds to a positive estuarine circulation, with freshwater flowing out through the surface layers and oceanic saline water entering through the deep layers. In addition, the rias circulation is highly dependent on wind regime. In the NW Iberian Peninsula, northerly winds at the shelf favor upwelling events and enhance positive estuarine circulation in the rias (Alvarez et al., 2005, 2008; Alvarez-Salgado et al., 1993; Barton et al., 2015; Gomez-Gesteira et al., 2006). Conversely, southerly winds induce downwelling events which have the ability to reverse the typical circulation pattern favoring freshwater to reach the deeper layers (Barton et al., 2015; deCastro et al., 2000; Des et al., 2019).

In the Rías Baixas, the tides are semi-diurnal and the tidal regime is mesotidal, with mean tidal amplitudes ranging between 1.3 m at neap tides and 3.4 m at spring tides in the Vigo harbor (http://www.puertos.es). Typical tidal current velocities are 5 cm s^{-1} for deep and 2 cm s^{-1} for shallow waters (Fanjul et al., 1997).

The main rivers flowing into the Rías Baixas are the Tambre River (Ría de Muros), the Ulla and Umia rivers (Ría de Arousa), the Lerez (Ría de

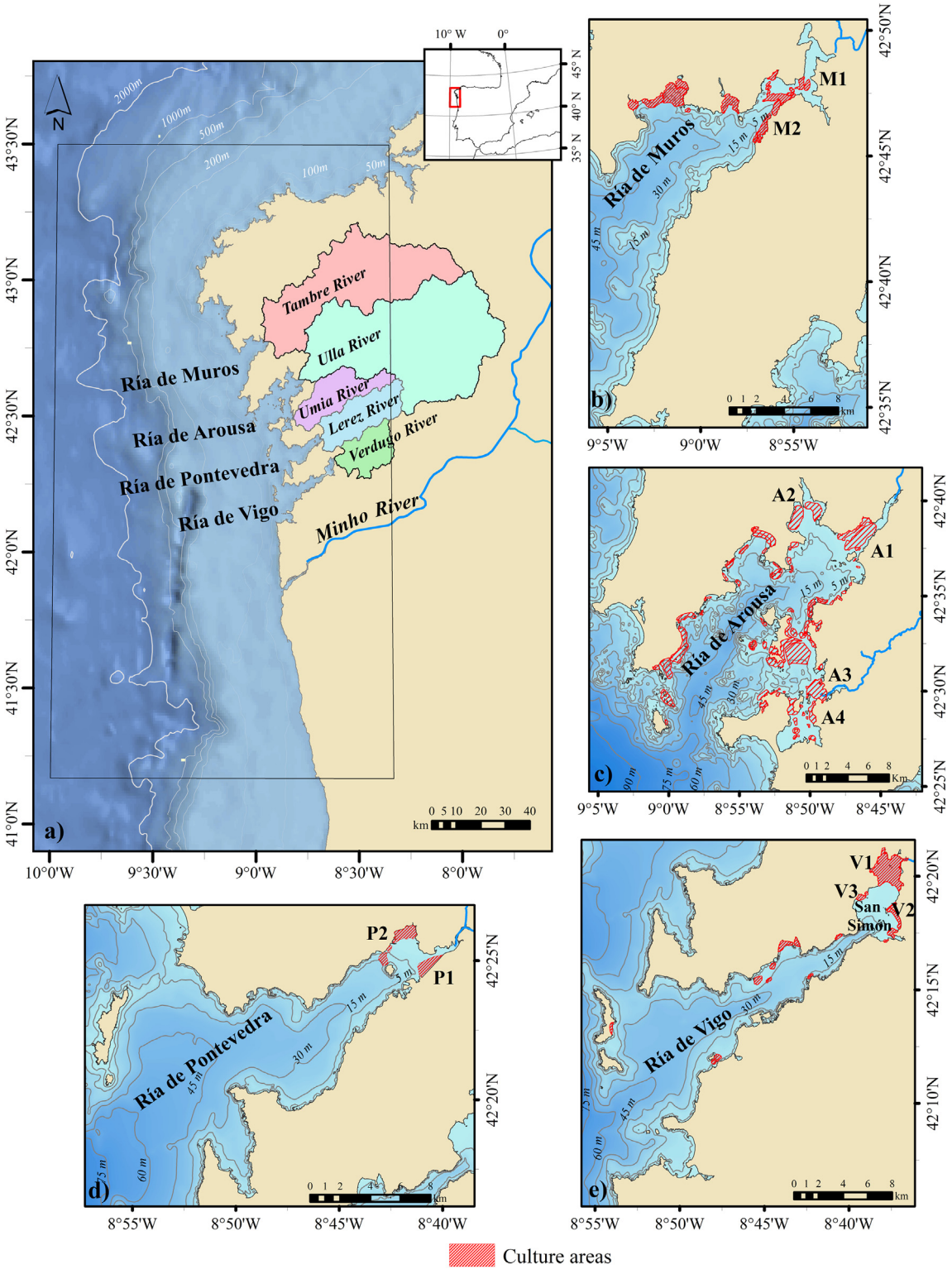

Fig. 1. (a) Location of the study area along the northwestern coast of the Iberian Peninsula. The box indicates the modeled area using Delft3D-Flow. Colored areas represent the river basins. Close-up view of the Ria de Muros (b), the Ría de Arousa (c), the Ría de Pontevedra (d) and the Ría de Vigo (e) showing the culture areas of *C. edule*, *R. decussatus*, *R. philippinarum* and *V. corrugata*.

Pontevedra) and the Verdugo River (Ría de Vigo). These rivers present an annual discharge ranging between 16.4 $m^3 s^{-1}$ for Umia River to 79.3 $m^3 s^{-1}$ for Ulla River (Table 1) and present a seasonal regime with maximum discharge during winter months (Sousa et al., 2014).

The main characteristics of the rias and river basins are summarized in Table 1.

3. Methodology

The following subsections describe the methodology carried out to evaluate the mortality of intertidal bivalve species of commercial interest due to the drop in salinity caused by extreme precipitation events for the historical (1990–2019) and future (2070–2099) periods. The

Table 1
Main characteristics of the rias and their fluvial inputs.

Rias	Area (km^2)	Volume (km^3)	Main river(s)	Catchment area (km^2)	Mean river(s) discharge ($m^3\ s^{-1}$)
Ría de Muros	125	2.1	Tambre	1561	54.10
Ría de Arousa	230	4.5	Ulla	2769	79.30
			Umia	445	16.39
Ría de Pontevedra	141	3.5	Lerez	449	21.21
Ría de Vigo	176	3.1	Verdugo	331	17.00

methodology can be summarized in: i) evaluating extreme precipitation data from CORDEX, ii) transforming the precipitation data provided by CORDEX for each basin into river discharge by means of a hydrological model, iii) modeling estuarine salinity by means of a hydrodynamic model using as inputs the river discharge calculated in previous item, atmospheric data from CORDEX and oceanic data from CMIP and iv) evaluating bivalve mortality based on lethal physiological thresholds of the species. A flowchart of the methodology can be found in supplementary material (Fig. S1).

3.1. Extreme precipitation events

Daily precipitation data with a spatial resolution of 0.11° were retrieved from the Regional Climate Models (RCMs) simulations performed within the framework of the CORDEX initiative (http://www.euro-cordex.net/). Currently, the EURO-CORDEX initiative offers more than 30 RCMs simulations corresponding to the RCP8.5 greenhouse gas emission scenario (Table 2, to facilitate the follow-up of this manuscript, a number has been assigned to each model given the complexity of the names of the models). The capability of the RCMs to reproduce the precipitations over the wet season (November to March) in the area under study was evaluated by comparing data from the historical simulations of each model against field data from pluviometers obtained from Meteogalicia database (www.meteogalicia.gal). This comparison was made by analyzing the entire distribution of the precipitation data (Perkins test) and extreme events (those that exceed the 99th percentile, P^{99} test). Only models with a Perkins test above 90% and P^{99} inside the range delimited by the 99th percentile of the mean precipitation of *in situ* data ± the standard deviation were considered in the further analysis (they are highlighted in bold in Table 2). In addition, results from the P^{99} test can be seen in Fig. S2 of supplementary material.

A three-point moving average of 3 days (using the previous and following day) was applied to the daily precipitation series following previous research by Cabalar (2005). This author observed that extreme precipitation events, caused by southwest winds, are normally associated with the passage of consecutive fronts for 3–4 days. The resulting series were used to calculate the mean precipitation over the wet season and precipitation for 10-year and 50-year return periods based on the Gumbel curve method (Yue et al., 1999; Kotz and Nadarajah, 2000; Onen and Bagatur, 2017). This procedure was carried out for the major rivers considering both the historical (1990–2019) and future (2070–2099) periods under study.

Table 2
Regional climate models (RCMs) driven by global climate models (GCMs) obtained from the EURO-CORDEX program. Each RCM has been assigned a number. Perkins' test column shows the models with skills greater than 90% to reproduce *in situ* values over the wet season (NDJFM) from the Perkins' test. P^{99} column shows the models with extreme precipitations (above the 99th percentile) inside the *in situ* mean values ± std. Models fulfilling both conditions are marked in bold.

#	Global//regional climate model	Perkins' test (%)	P^{99}
1	**CNRM-CERFACS-CNRM-CM5_CLMcom//CCLM4-8-17**	**93**	**Yes**
2	CNRM-CERFACS-CNRM-CM5_RMIB-UGent//ALARO-0	–	–
3	CNRM-CERFACS-CNRM-CM5_SMH//RCA4	–	–
4	ICHEC-EC-EARTH_CLMcom//ETH-COSMO-crCLIM-v1-1	93	–
5	ICHEC-EC-EARTH_DMI//HIRHAM5	94	–
6	**ICHEC-EC-EARTH_KNMI//RACMO22**	**91**	**Yes**
7	ICHEC-EC-EARTH_SMHI//RCA4	–	–
8	IPSL-IPSL-CM5A-MR_DMI//HIRHAM5	–	–
9	IPSL-IPSL-CM5A-MR_GERICS//REMO2015	–	–
10	IPSL-IPSL-CM5A-MR_IPSL-INERIS//WRF331F	–	–
11	IPSL-IPSL-CM5A-MR_KNMI//RACMO22E	–	–
12	IPSL-IPSL-CM5A-MR_SMH//RCA4	–	–
13	**MOHC-HadGEM2-ES_CLMcom//CCLM4–8-17**	**93**	**Yes**
14	MOHC-HadGEM2-ES_CLMcom//ETH-COSMO-crCLIM-v1-1	93	–
15	MOHC-HadGEM2-ES_CNRM//ALADIN63	–	–
16	MOHC-HadGEM2-ES_ICTP//RegCM4-6	–	Yes
17	MOHC-HadGEM2-ES_SMHI//RCA4	–	–
18	**MPI-M-MPI-ESM-LR_CLMcom//CCLM4-8-17**	**91**	**Yes**
19	MPI-M-MPI-ESM-LR_CLMcom//ETH-COSMO-crCLIM-v1-1	93	–
20	MPI-M-MPI-ESM-LR_CNRM//ALADIN63	–	–
21	MPI-M-MPI-ESM-LR_DMI//HIRHAM5	–	–
22	MPI-M-MPI-ESM-LR_ICTP//RegCM4-6	–	Yes
23	MPI-M-MPI-ESM-LR_KNMI//RACMO22E	–	–
24	MPI-M-MPI-ESM-LR_MPI-CSC//REMO2009	–	–
25	MPI-M-MPI-ESM-LR_SMHI//RCA4	–	–
26	NCC-NorESM1-M_CLMcom//ETH-COSMO-crCLIM-v1-1	93	–
27	NCC-NorESM1-M_CNRM//ALADIN63	–	–
28	NCC-NorESM1-M_GERICS//REMO2015	–	–
29	**NCC-NorESM1-M_IPSL//WRF381P**	**93**	**Yes**
30	NCC-NorESM1-M_KNMI//RACMO22E	–	–
31	NCC-NorESM1-M_SMHI//RCA4	–	–

3.2. Hydrological model

The semi-distributed model HEC-HMS (Feldman, 2000; Scharffenberg et al., 2018; U.S. Army Corps of Engineers, 2018), was used to model the hydrological process for the river basins under analysis. This modeling system, which is one of the most used for hydrological procedures worldwide, have shown accurate results for nearby areas (Cea and Fraga, 2018; Fernández-Nóvoa et al., 2020; Fraga et al., 2020; González-Cao et al., 2019). In order to convert the precipitation events on the respective river flow, loss (infiltration) and transformation processes were taken into account. In the first case, the Soil Conservation Service (SCS) curve number method was selected to calculate the infiltration capability of the selected areas, providing the excess rainfall which is subject to surface runoff. Then, the SCS unit hydrograph method was selected to transform this excess rainfall into runoff. In this sense, the lag time, the parameter which modulates the transformation of excess rainfall into runoff, was calculated following the equation proposed by Spanish Development Ministry (Ministerio de Fomento, 2016), which provides a good approximation for Spanish basins:

$$T_l = 0.105 \cdot L_c^{0.76} \cdot J_c^{-0.19}$$

where L_c is the length of the longest flow channel (km) and J_c is its corresponding slope (m/m). The topographic data were obtained from digital terrain models from the National Geographical Institute (www.ign.es/web/ign/portal).

Curve number (CN) for each basin was calibrated under high river discharge conditions by means of the specific calibration tools implemented in HEC-HMS using river flow obtained from Meteogalicia database. The CN values obtained for the precipitation conditions considered in the study ranged from 87 to 94. These values are similar to those obtained in previous studies developed in close areas corresponding to moist soil conditions (soils highly saturated), the most critical situation from the point of view of extreme river discharge events (Cea and Fraga, 2018; Fernández-Nóvoa et al., 2020; González-Cao et al., 2019).

The discharge of the main rivers was calculated for each return period based on the precipitation data obtained from each RCM for historical and future periods (Fig. S3 and Fig. S4 of supplementary material).

3.3. Hydrodynamic model

Delft3D-Flow was used to compute salinity within the Rías Baixas under extreme precipitation events. The model configuration used

(computational grid, parametrization and implementation) was previously calibrated and validated by Des et al. (2019, 2020a, b), where a more detailed description of parametrization calibration can be found.

The mesh covers from 8.33° W to 10.00° W and from 41.18° N to 43.50° N (Fig. 1a, rectangle). The resolution varies, being approximately 2200 m × 800 m on the west boundary and gradually increasing towards onshore, allowing higher resolution in the rias (220 m × 140 m) and the Minho estuary (50 m × 77 m). The high spatial resolution in the rias allows Delft3D-flow to provide, among other variables, salinity data in the areas of the Rías Baixas where the species of interest (*V. corrugata*, *C. edule*, *R. decussatus* and *R. philippinarum*) are gathered. The vertical resolution of the model was defined as 16 sigma layers with top and deep layers refined.

The bathymetric input for the model simulations was created from compiling data from different sources. Data of Ría de Muros, Ría de Arousa and the adjacent shelf area were obtained from nautical charts of the Spanish Navy Hydrographical Institute. Data of the rias of Pontevedra and Vigo were provided by the General Fishing Secretary. Data of the Minho estuary were provided by the Portuguese Navy Hydrographic Institute. Gaps in the dataset were filled using data from the General Bathymetric Chart of the Oceans (GEBCO, https://www.gebco.net/).

The oceanic boundary was forced with transport conditions (salinity and water temperature) and water level. Transport conditions were retrieved from the MOHC-HadGEM2-Es GCM outputs (https://esgf-node.ipsl.upmc.fr/projects/esgf-ipsl/), following Des et al. (2020a, 2020b) and Sousa et al. (2020). Tidal harmonic constituents (M2, S2, N2, K2, K1, O1, P1, Q1, MsF, MM, M4, MS4, MN4) obtained from the model TPXO 7.2 TOPEX/Poseidon Altimetry (http://volkov.oce.orst.edu/tides/global.html) were prescribed as astronomical forcing. Atmospheric conditions were imposed using the "absolute flux, net solar radiation" model, which requires relative humidity, air temperature and the combined net solar (short wave) and net atmospheric (longwave) radiation. Wind components and pressure values were imposed varying spatially. Atmospheric data were retrieved from the MOHC-HadGEM2-Es-RCA4 RCM outputs (http://www.cordex.org/) also following Des et al. (2020a, 2020b) and Sousa et al. (2020).

River discharges for the main tributaries in the Rías Baixas and Minho River were imposed in the model as fluvial open boundaries. These discharges data were calculated using the HEC-HMS hydrological model.

3.3.1. Numerical scenarios

Numerical scenarios were defined in order to determine salinity variations as a function of the return period of precipitations events (10-year and 50-year return period), tidal influence (spring and neap tides) and RCM for historical (1990–2019) and future (2070–2099) periods. Thus, a total of 40 numerical scenarios were run.

Transport conditions at the open boundary were determined through the computation of climatological mean for the winter months, when the extreme precipitation events take place. The same procedure was carried out for the atmospheric variables except for the wind that deserves a detailed analysis since it is strongly linked to the passage of fronts. Previous studies in the area under scope (Sousa et al., 2020) showed that MOHC-HadGEM2-Es-RCA4 is the best RCM to reproduce historical climate conditions in the region. According the statistical analysis obtained from the MOHC-HadGEM2-Es-RCA4 RCM outputs, shows that the typical wind pattern in winter corresponds to a mean intensity of 8.4 m s^{-1} (historical period) and 7.9 m s^{-1} (future) with a variable direction, where all sectors in the wind rose show a similar probability. In addition, the passage of fronts is characterized by southwesterly winds with higher intensity. In particular, the wind intensities corresponding to the 90th percentile were considered with values of 14.3 m s^{-1} and 13.9 m s^{-1} for historical and future periods, respectively.

Each simulation comprised a 40-day run, 30 days of spin-up and 10 days corresponding to the event. During the spin-up period, typical wind speed for historical (8.4 m s^{-1}) and for the future (7.9 m s^{-1}) periods was imposed as constant while wind direction varies in clockwise direction changing 45° h^{-1}. This approach, which was previously used in Sousa et al. (2020), allows activating the heat diffusion processes between the ocean and the atmosphere without imposing a dominant surface-wind pattern. River discharges calculated from average winter rainfall were imposed. The event starts after the spin-up period, during the first three days a wind speed corresponding to the 90th percentile (14.3 m s^{-1} for the historical period and 13.9 m s^{-1} for future) and a southwest direction was imposed to mimic the passage of fronts. Then, on day four, the wind pattern used in the spin-up is resumed. During the whole event, the river discharges calculated for each return period were imposed (Fig. 2, the blue lines represent river discharges for the historical period and red lines those for the future period). Finally, the peak of river discharges was imposed to coincide with spring or neap tides, to evaluate the effect of tides on mortality.

3.4. Mortality predictor

Salinity drops below the lethal physiological threshold of the species are the main factor causing mortality of *V. corrugata*, *C. edule*, *R. decussatus* and *R. philippinarum* during extreme precipitation events. According to META database (Maritime and Environmental Thresholds for Aquaculture, https://longline.co.uk/meta/Litt), the low lethal physiological threshold of *V. corrugata* is 7 with optimal salinity ranges between 14 and 28; for *C. edule* the low lethal physiological threshold is 12.5 and the optimal salinity ranges between 20 and 25; for *R. decussatus* the low lethal physiological threshold is 3 and the optimal salinity ranges between 20 and 28, and for *R. philippinarum* the low lethal physiological threshold is 7 and the optimal salinity ranges between 20 and 30. Due to the mechanisms of resistance and tolerance of the species, drops in salinity below the optimal or even lethal physiological threshold do not have an instant effect, being necessary to maintain salinity low over time. Therefore, mortality of *V. corrugata*, *C. edule*, *R. decussatus* and *R. philippinarum* was assessed following the results of Parada et al. (2012), who categorize the mortality episodes according to the daily average value of salinity in a determined time, being able to stipulate the percentage of death for each species as follows: i) severe mortality, mortality rates of at least 50% for *C. edule* or *V. corrugata* and ≥15% for *R. decussatus* and/or *R. philippinarum*, which occurs when daily mean salinity at the seabed remains below 10 for at least 7 days or below 15 for at least 9 days; and ii) moderate mortality, mortality lower than 50% for *C. edule*, very high mortality for *V. corrugata* and <15% for *R. decussatus* and/or *R. philippinarum*, which occurs when mean bottom salinity remains below 15 for at least 3 consecutive days or below 10 for at least 1 day. The thresholds are in agreement with those obtained by Verdelhos et al. (2015) on laboratory assays.

Firstly, bivalve mortality was calculated according to salinity results obtained from each of the 40 numerical scenarios. Thus, five maps were obtained for each study case, one for each RCM. To compile the results, each cell of the map was analyzed and categorized according to the mode, the agreement between models is never less than 60% (see supplementary material, Figs. S5 to S8).

4. Results and discussion

4.1. Precipitations and hydrological model

As mentioned above, a Perkins test was carried out to analyze the most accurate models to reproduce the past rain conditions in the area (Table 2). A good fit, considered as a skill greater than 90%, was obtained for models #1, #4, #5, #6, #13, #14, #18, #19, #26 and #29. In addition, the P^{99} test was passed by models #1, #6, #13, #16, #18, #22 and #29. Thereby, the models that pass both tests are #1, #6, #13, #18 and #29. Consequently, these models were used to calculate the mean precipitation over the wet season and the extreme

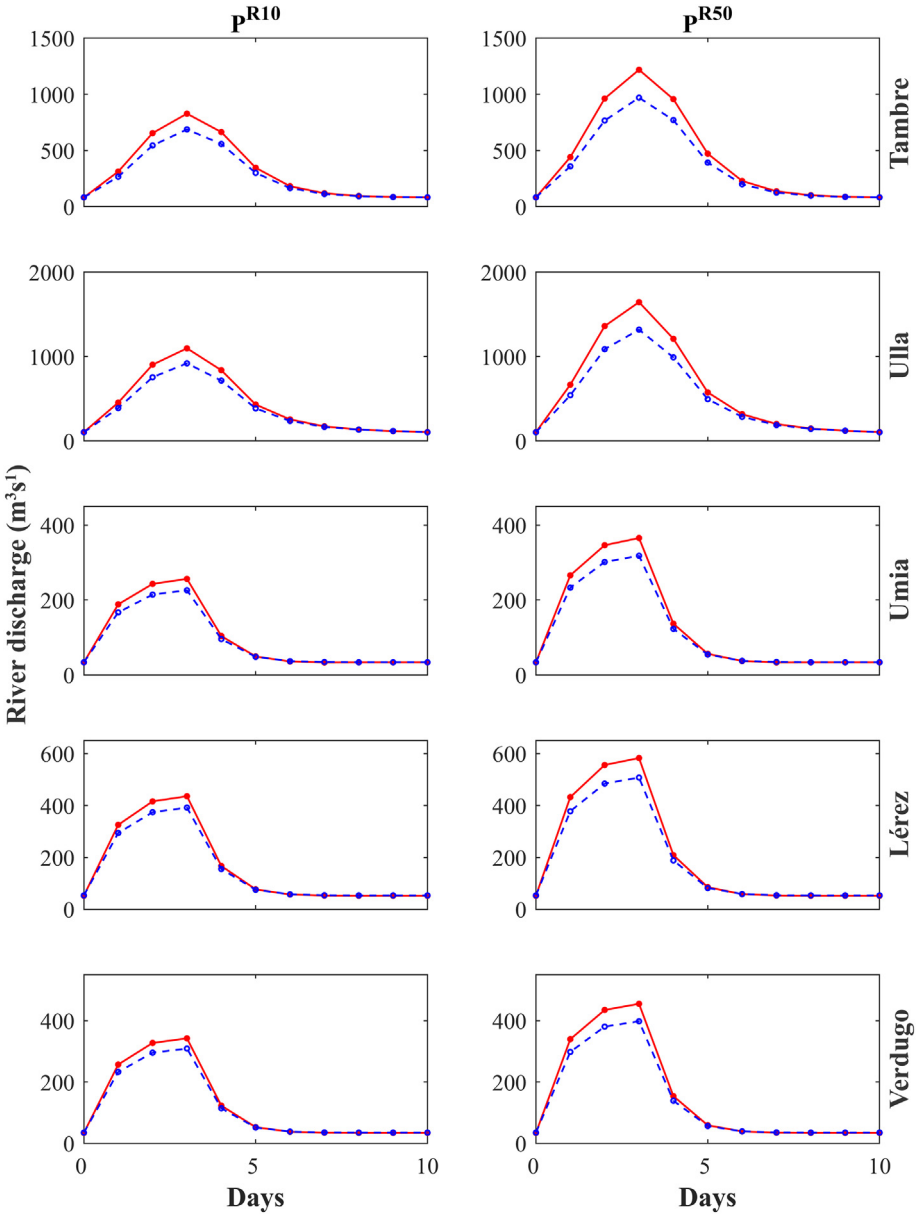

Fig. 2. River discharge calculated from precipitation events for a return period of 10-year (left panel) and 50-year (right panel) averaged to all RCMs. Blue line represent the river discharge calculated for the historical period. Red line represent the river discharge calculated for the future period. (For interpretation of the references to color in this figure legend, the reader is referred to the web version of this article.)

precipitation for 10-year (P^{R10}) and 50-year (P^{R50}) return periods for each of the basins (Table 3). In general, results show negligible variations in the mean precipitation in all basins over the wet season and an increase in future extreme precipitations, of around 13% for P^{R10} and around 15% for P^{R50}. In general, there is an agreement between models in predicting an increase in future precipitation with small discrepancies. Only, model #29 predicts a decrease in future precipitation.

The discharge curve for the main rivers flowing into the Rías Baixas was calculated for each model and return period by means of the hydrological model HEC-HMS using the respective precipitation obtained in Table 3. These river discharge curves are represented in Figs. S3 and S4 of the supplementary material. Additionally, the model average of the river discharges represented in Fig. 2 show, as expected, that the longer the return period the higher the discharge peaks. Extreme river discharges will increase by the end of the century in all basins. The obtained results are in good agreement with previous research. For example, mean Tambre River flow calculated from the historical 50-year return period presents a peak slightly above 1000 $m^3\ s^{-1}$ in agreement with peak values detected by Martínez-Conde et al. (2000) and with historical data obtained from CEDEX (Centro de Estudios y Experimentación de Obras Públicas, ceh.cedex.es). In addition, the CEDEX database shows Lerez River peak values that surpass 300 $m^3\ s^{-1}$ during the last decade, which are similar to the mean value calculated for the historical 10-year return period.

4.2. Mortality predictor

The areas where bivalves of commercial interest can be potentially affected by mortality during extreme precipitation events are shown in Fig. 3. Calculations were carried out for the historical period (1990–2019) and the future (2070–2099) under the RCP 8.5 greenhouse gas emission scenario using the numerical scenarios described above. In particular, the case depicted in this figure corresponds to a return period of 50 years under neap tides.

The areas closest to the river mouths are the most affected by mortality events. The shape of these areas tends to follow the spatial

Table 3
10-Return period precipitation (P^{R10}), 50-return period precipitation (P^{R50}) and mean precipitation ($\overline{P}$) from each RCM calculated for each river basin by accumulating three days, one before and one after of the analyzed day, for historical and future periods.

Basin	Variable	#1		#6		#13		#18		#29	
		H	*F*	H	*F*	H	*F*	H	*F*	H	*F*
Tambre	P^{R10}	59	*60*	57	*66*	63	*71*	66	*84*	46	*53*
	P^{R50}	78	*77*	72	*87*	86	*100*	82	*113*	59	*73*
	$\overline{P}$	7.2	*7.2*	8.3	*8.6*	5.9	*5.5*	9.6	*10.3*	6.1	*5.4*
Ulla	P^{R10}	52	*59*	58	*59*	60	*74*	68	*88*	49	*45*
	P^{R50}	66	*77*	76	*75*	79	*103*	86	*120*	65	*61*
	$\overline{P}$	7.2	*6.9*	7.5	*7.7*	5.8	*5.5*	9.6	*10.1*	5.9	*5.3*
Umia	P^{R10}	63	*68*	77	*89*	69	*77*	79	*97*	65	*56*
	P^{R50}	80	*88*	98	*116*	93	*102*	100	*129*	84	*73*
	$\overline{P}$	8	*7.8*	10.3	*10.5*	6.5	*6.3*	11	*11.8*	8.5	*7.8*
Lerez	P^{R10}	63	*71*	88	*86*	76	*97*	82	*101*	73	*68*
	P^{R50}	77	*93*	112	*109*	100	*135*	101	*131*	98	*90*
	$\overline{P}$	9	*8.5*	11.4	*11.5*	7.2	*7*	12.4	*12.9*	8.6	*7.6*
Verdugo	P^{R10}	70	*79*	92	*91*	81	*97*	88	*110*	79	*78*
	P^{R50}	87	*105*	117	*114*	108	*133*	109	*144*	106	*106*
	$\overline{P}$	9.4	*8.9*	12.1	*12.1*	7.4	*7.2*	13	*13.4*	9.2	*8.1*

distribution of the river plumes, which normally flow parallel to the northern shore (Alvarez et al., 2005). Although the presence of freshwater tends to be limited to the surface layer due to the two-layered circulation pattern (Taboada et al., 1998), extreme precipitation events associated with southwesterly winds favor the accumulation of freshwater near bed (Barton et al., 2015; deCastro et al., 2000; Des et al., 2019), which worsens the conditions for the survival of the species analyzed (Parada et al., 2012). Consequently, salinity drop at bottom layers, which can potentially cause mortality, is mainly restricted to shallow areas near the river mouth.

Fig. 3 shows a qualitative increment in the extent of the area affected by mortality in the future. A quantitative comparison between the future and historical extent of the mortality areas for a return period of 50 years is shown in Tables 4 and 5 under spring and neap tides, respectively. Results are similar for the rest of cases (see Figs. S9–S11 and Tables S1 and S2 in supplementary material).

For the historical period the Ría de Arousa, where shellfish production is higher, is the most affected by total mortality under both tidal conditions. This is consistent with the hydrography of the ria, as the Ulla River, the largest river flowing into the Rías Baixas, and the Umia River flow into the Ría de Arousa providing the largest inflow of freshwater. The Ría de Muros is the second most affected area by severe mortality where the Tambre River is located, the second largest river in the area. At Ulla (Ría de Arousa) and Tambre (Ría de Muros) river mouths, the area affected by mortality for 50-year return period precipitation events seems to be related with the bathymetry (Fig. 3). The outer limit of the area affected simulates the shape of the 5-m-contour-bathymetry line, never reaching it. In spite of the rias of Pontevedra and Vigo have similar hydrology and fresh water input the impact of extreme discharge on mortality are different (Fig. 3, Tables 4 and 5). In the Ría de Pontevedra, the area affected by mortality is small, without severe mortality events (Tables 4 and 5). In contrast, mortality in the Ría de Vigo affects a large part of the San Simón Bay (Tables 4 and 5 and Fig. 3). This different behavior is probably due to the different physiography of the rias. Although both rias share some common features, as mentioned above, they differ mainly in the inner part where the Ría de Pontevedra is characterized by a progressive widening while the Ría de Vigo presents an inlet, the San Simón Bay (Fig. 1e). It constitutes a shallow area of low hydrodynamic energy connected to the outer ria through a narrow channel (Álvarez-Iglesias et al., 2003; Iglesias and García-Gil, 2007). On the other hand, the inner part of the Ría de Pontevedra is directly connected with the outer ria following the same orientation and is generally deeper than San Simón bay, being the intertidal area less extensive and restricted to the zone near the Lerez River mouth. In summary, bathymetry is a fundamental factor to modulate the mortality area. On the one hand, depth limits the affected areas as freshwater is not able to reach the bottom and, on the other hand, the presence of embayments can also affect freshwater distribution.

The extent of the area affected by mortality is larger under neap tides, possibly due do the fact that spring conditions tend to dilute the freshwater plume faster. During spring tides, current velocities are stronger and oceanic water fluxes dominate over the river flow in intertidal zones. Moreover, although larger areas become exposed during low tides due to the higher tidal range, oceanic salt water covers a larger area during flood increasing salinity at the bottom. Conversely, during neap tidal cycles, the influence of ocean water is reduced and the fluvial discharge dominates, keeping the salinity values low for a longer time and in a larger area. In this sense, it can be concluded that the coincidence of extreme precipitation events with neap tides is detrimental to the gathering of the studied species. These results agree with those obtained by Parada et al. (2012) who observed that the coincidence of freshwater input and large tidal amplitudes might be less critical to the species survival.

When focusing on the future increment, the extent of the total area affected by mortality will increase under both tidal conditions (last column in Tables 4 and 5). The same behavior is observed for the area affected by severe mortality. The extent of the area affected by moderate mortality could diminish in the future for some rias, especially under neap tides. This decrease is only apparent, since it corresponds to the worsening in mortality conditions that evolve from moderate to severe. The future increase in extreme precipitation will lead to a higher river discharges and, therefore, to a greater inflow of freshwater into the rias, leading to a decrease in salinity and worsening the environmental conditions to which bivalves are exposed. Thus, future conditions will be less favorable for species like *V. corrugata*, *C. edule*, *R. decussatus* and *R. philippinarum*.

A detailed analysis of the projected changes was carried out from 11 currently existing gathering areas near river mouths, which may be affected by mortality events (marked with M or S in Tables 6 and 7). In general, the number of collection plots affected by mortality increases with the return period of extreme precipitations, independently of the tidal conditions. This increase is observed both for the historical period (from 5 to 7 plots affected under spring tides and from 6 to 10 plots under neap tides) and for the future period (from 6 to 8 under spring tides and from 8 to 11 under neap tides). In addition, future mortality conditions will never be better than observed for the historical period, regardless of the return period or the tidal conditions. This is especially true for the 50-year return period, where future conditions will worsen compared to the historical period in 3 collection plots under spring tides (M1, A3, P2) and neap tides (M2, A4, P2, V1). Note that the plots affected under spring and neap tides are different, thus, future conditions will be worse in 6 out of 11 collection plots (M1, M2, A3, A4, P2, V1) when

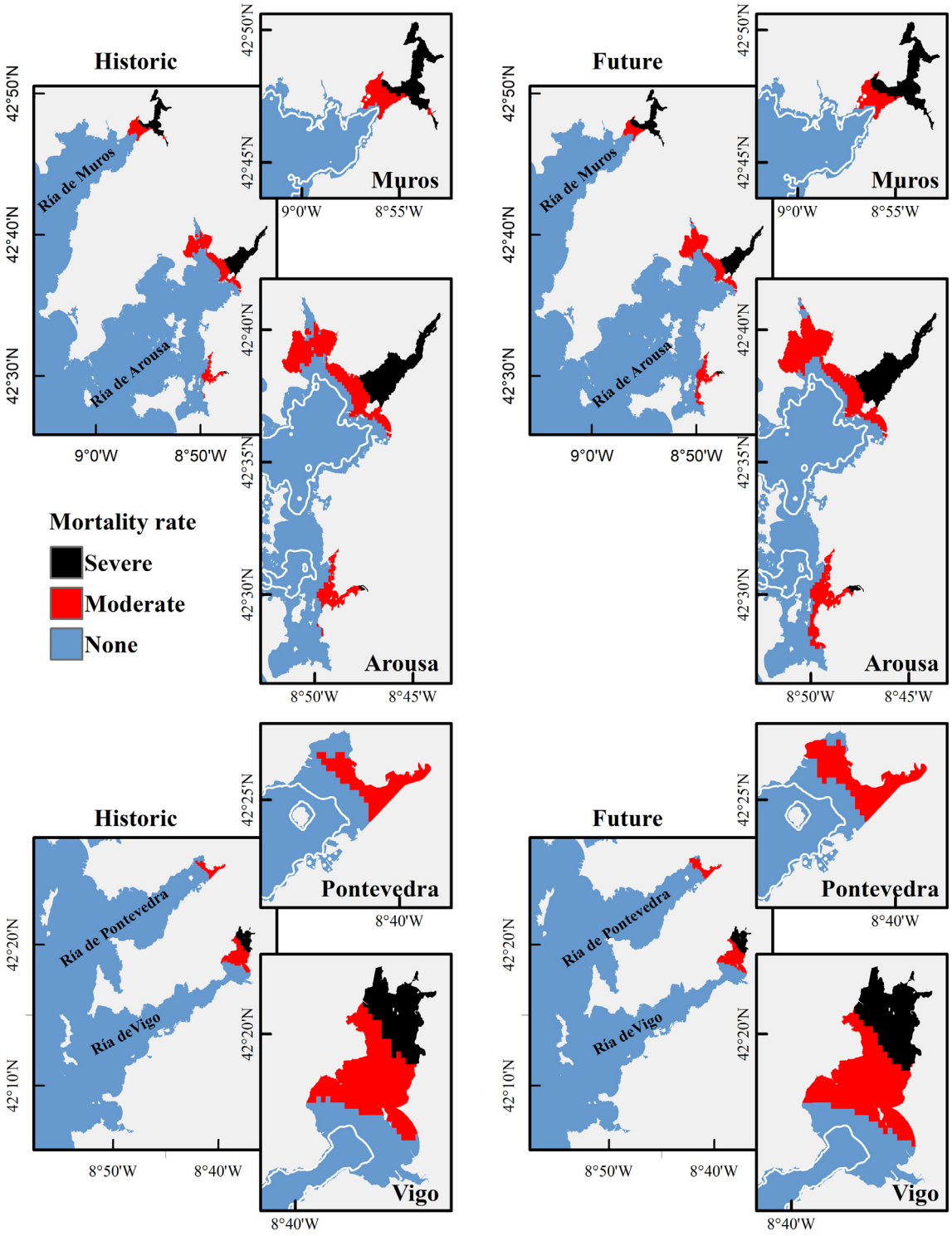

Fig. 3. Areas affected by serious mortality (black) and moderate mortality (red) based on modeled salinity for historic (1990–2019) and future (2070–2099) 50-year return period precipitation events under neap tides. Five meters contour bathymetry line is shown in white. (For interpretation of the references to color in this figure legend, the reader is referred to the web version of this article.)

taking into account both tidal conditions. A similar behavior is observed for 10-year return period although at a lesser extent, since conditions will be worse in 2 plots (A2 and V3).

5. Conclusions

The historical and future mortality of species such as *V. corrugata*, *C. edule*, *R. decussatus* and *R. philippinarum* in the Rías Baixas has been analyzed. This mortality due to the decrease in salinity caused by extreme precipitation events has been analyzed under both historical and future precipitation established by the RCP8.5 scenario, taking into account different return periods (10 and 50 years).

Under a business-as-usual pathway, future moderate and severe mortality conditions due to extreme rainfall will be worse than historically observed. This worsening is reflected both in the extension of the

Table 4
Occurrence of severe and moderate mortality for the studied species under extreme discharges and spring tides for 50-year return period. The extent of the area (km^2) affected by mortality for the historic period (1990–2019) and the increment (difference between future and historical conditions) for the future period (2070–2099) are shown.

Ria	Historical area (km^2)			Increment of area (km^2)		
	Moderate	Severe	Total	Moderate	Severe	Total
Muros	7.98	6.14	14.11	−0.06	0.50	0.44
Arousa	14.76	6.53	21.29	1.77	0.52	2.29
Pontevedra	1.16	0.00	1.16	1.55	0.00	1.55
Vigo	8.54	1.41	9.95	0.64	0.22	0.86

Table 5
Occurrence of severe and moderate mortality for the studied species under extreme discharges and neap tides for 50-year return period. The extent of the area (km^2) affected by mortality for the historic period (1990–2019) and the increment (difference between future and historical conditions) for the future period (2070–2099) are shown.

Ria	Historical area (km^2)			Increment of area (km^2)		
	Moderate	Severe	Total	Moderate	Severe	Total
Muros	4.97	9.77	14.74	−1.14	1.24	0.10
Arousa	16.67	8.12	24.79	3.70	0.39	4.10
Pontevedra	2.41	0.00	2.41	0.90	0.00	0.90
Vigo	7.49	5.10	12.59	−0.09	0.54	0.45

affected area and in the impact on areas where collection plots already exists today.

Future increase in the mortality conditions will be more intense and will cover a larger area under neap tides. This fact seems to be due to a higher dilution of the fresh water plume under spring tides. In addition, the areas affected by extreme discharges can be different under both tidal conditions, in such a way that future conditions will be worse in 6 out of 11 collection plots under analysis when both spring and neap tides are considered.

Although all the Rías Baixas will be potentially affected, the impact will be different for each ria. Thus, Arousa, which is the ria with the highest production of species such as *V. corrugata*, *C. edule*, *R. decussatus* and *R. philippinarum*, has the largest affected area for the historical period and the greatest deterioration in the future. In contrast, the Muros ria, which is the second in terms of extension of the affected area for the historical period, has an almost insignificant increase in the future. Finally, Pontevedra and Vigo have similar freshwater inputs but the extent of the affected area and its future increase is completely different. This implies that apart from precipitation and tidal conditions, bathymetric and topographic features must also be taken into account.

Table 6
Predicted mortality for the studied species in growing areas affected by extreme precipitation events for historic (1990–2019) and future (2070–2099) period under spring tides.

Cultivation plot	P^{R10}		P^{R50}	
	H	F	H	F
M1	M	M	M	M/S
M2	N/M	N/M	N/M	N/M
A1	M/S	M/S	M/S	M/S
A2	N	M	M	M
A3	N	N	N/M	M
A4	N	N	N	N
P1	N/M	N/M	N/M	N/M
P2	N	N	N	M
V1	M*	M*	M*	M*
V2	N	N	N*	N*
V3	N	N	N	N

S severe mortality, M, moderate mortality and N no mortality due to salinity drops. S* it means that almost the entire growing area is under conditions of severe mortality. Areas where changes between historical and the future are observed have been highlighted.

Table 7
Predicted mortality for the studied species in growing areas affected by extreme precipitation events for historic (1990–2019) and future (2070–2099) period under neap tides.

Cultivation plot	P^{R10}		P^{R50}	
	H	F	H	F
M1	S	S	S	S
M2	N/M	N/M	N/M	N/M/S
A1	S	S	S	S
A2	N/M	M	M	M
A3	M	M	M	M
A4	N	N	N	M
P1	N/M	N/M	M	M
P2	N	N	N/M	M
V1	M/S	M/S	M/S	S*
V2	N	N	N/M	N/M
V3	N	M	M	M

S severe mortality, M, moderate mortality and N no mortality due to salinity drops. S* it means that almost the entire growing area is under conditions of severe mortality. Areas where changes between historical and the future are observed have been highlighted.

CRediT authorship contribution statement

M. Des: Conceptualization, Methodology, Software, Visualization, Writing – original draft, Investigation, Writing – review & editing. **D. Fernández-Nóvoa:** Conceptualization, Methodology, Software, Visualization, Investigation, Writing – review & editing. **M. deCastro:** Conceptualization, Methodology, Software, Visualization, Investigation, Writing – review & editing, Supervision, Funding acquisition. **J.L. Gómez-Gesteira:** Conceptualization, Methodology, Software, Investigation, Writing – review & editing. **M.C. Sousa:** Investigation, Writing – review & editing. **M. Gómez-Gesteira:** Conceptualization, Methodology, Software, Visualization, Investigation, Writing – review & editing, Supervision, Funding acquisition.

Declaration of competing interest

The authors declare that they have no known competing financial interests or personal relationships that could have appeared to influence the work reported in this paper.

Acknowledgements

The authors thank the Confederación Hidrográfica Miño-Sil, MeteoGalicia and the Hype Web portal for the distribution of river discharge data, the Copernicus Marine Service website for the distribution of IBI data, the General Fishing Secretary, the Spanish Navy Hydrographical Institute and General Bathymetry Chart of the Oceans for the bathymetry data, the WCRP's Working Group on Regional Climate, and the Working Group on Coupled Modeling, former coordinating body of CORDEX and responsible panel for CMIP5. We also thank the climate modeling groups for producing and making available their models' outputs that can be downloaded at http://www.cordex.org/.

MCS was supported by national funds (OE), through FCT, I.P., in the scope of the framework contract foreseen in the numbers 4, 5 and 6 of the article 23, of the Decree-Law 57/2016, of August 29, changed by Law 57/2017, of July 19.

This work was partially financed by Xunta de Galicia (Spain) under project ED431C 2017/64 "Programa de Consolidación e Estructuración de Unidades de Investigación Competitivas". This work was also funded by European Regional Development Fund under Interreg project "MarRISK" (0262_MARRISK_1_E).

Thanks are due to FCT/MCTES for the financial support to CESAM (UIDP/50017/2020 + UIDB/50017/2020) through national funds.

Funding for open access charge: Universidade de Vigo/CISUG.

Appendix A. Supplementary data

Supplementary data to this article can be found online at https://doi.org/10.1016/j.scitotenv.2021.148147.

References

Aguiar, E., Piedracoba, S., Álvarez-Salgado, X.A., Labarta, U., 2017. Circulation of water through a mussel raft: clearance area vs. idealized linear flows. Rev. Aquac. 9, 3–22. https://doi.org/10.1111/raq.12099.

Algarra, I., Nieto, R., Ramos, A.M., Eiras-Barca, J., Trigo, R.M., Gimeno, L., 2020. Significant increase of global anomalous moisture uptake feeding landfalling atmospheric rivers. Nat. Commun. 11, 5082. https://doi.org/10.1038/s41467-020-18876-w.

Alvarez, I., deCastro, M., Gomez-Gesteira, M., 2005. Inter- and intra-annual analysis of the salinity and temperature evolution in the Galician Rías Baixas–ocean boundary (northwest Spain). J. Geophys. Res. 110. https://doi.org/10.1029/2004JC002504.

Alvarez, I., Gomez-Gesteira, M., deCastro, M., Novoa, E.M., 2008. Ekman transport along the Galician Coast (NW, Spain) calculated from QuikSCAT winds. J. Mar. Syst. 72, 101–115. https://doi.org/10.1016/j.jmarsys.2007.01.013.

Álvarez-Iglesias, P., Rubio, B., Vilas, F., 2003. Pollution in intertidal sediments of San Simon Bay (Inner Ria de Vigo, NW of Spain): total heavy metal concentrations and speciation. Mar. Pollut. Bull. 46, 491–503.

Alvarez-Salgado, X.A., Rosón, G., Pérez, F.F., Pazos, Y., 1993. Hydrographic variability off the Rías Baixas (NW Spain) during the upwelling season. J. Geophys. Res. 98, 14447. https://doi.org/10.1029/93JC00458.

Barton, E.D., Largier, J.L., Torres, R., Sheridan, M., Trasviña, A., Souza, A., Pazos, Y., Valle-Levinson, A., 2015. Coastal upwelling and downwelling forcing of circulation in a semi-enclosed bay: Ria de Vigo. Prog. Oceanogr. 134, 173–189. https://doi.org/10.1016/j.pocean.2015.01.014.

Berger, V.J., Kharazova, A.D., 1997. Mechanisms of salinity adaptations in marine molluscs. Interactions and Adaptation Strategies of Marine Organisms. Springer, pp. 115–126.

Cabalar, M., 2005. Los temporales de lluvia y viento en galicia. Propuesta de clasificación y análisis de tendencias (1961-2001). Incestigaciones Geográficas 36, 103–118. https://doi.org/10.14198/INGEO2005.36.03.

Cardoso Pereira, S., Marta-Almeida, M., Carvalho, A.C., Rocha, A., 2020. Extreme precipitation events under climate change in the Iberian Peninsula. Int. J. Climatol. 40, 1255–1278.

Carregosa, V., Velez, C., Soares, A.M., Figueira, E., Freitas, R., 2014. Physiological and biochemical responses of three Veneridae clams exposed to salinity changes. Comp. Biochem. Physiol. B: Biochem. Mol. Biol. 177, 1–9.

Cea, L., Fraga, I., 2018. Incorporating antecedent moisture conditions and intraevent variability of rainfall on flood frequency analysis in poorly gauged basins. Water Resour. Res. 54, 8774–8791.

deCastro, M., Gómez-Gesteira, M., Prego, R., Taboada, J.J., Montero, P., Herbello, P., Pérez-Villar, V., 2000. Wind and tidal influence on water circulation in a Galician Ria (NW Spain). Estuar. Coast. Shelf Sci. 51, 161–176. https://doi.org/10.1006/ecss.2000.0619.

Des, M., deCastro, M., Sousa, M.C., Dias, J.M., Gómez-Gesteira, M., 2019. Hydrodynamics of river plume intrusion into an adjacent estuary: the Minho River and Ria de Vigo. J. Mar. Syst. 189, 87–97. https://doi.org/10.1016/j.jmarsys.2018.10.003.

Des, M., Gómez-Gesteira, M., deCastro, M., Gómez-Gesteira, L., Sousa, M.C., 2020a. How can ocean warming at the NW Iberian Peninsula affect mussel aquaculture? Sci. Total Environ. 709, 136117. https://doi.org/10.1016/j.scitotenv.2019.136117.

Des, M., Martínez, B., deCastro, M., Viejo, R.M., Sousa, M.C., Gómez-Gesteira, M., 2020b. The impact of climate change on the geographical distribution of habitat-forming macroalgae in the Rías Baixas. Mar. Environ. Res. 161, 105074. https://doi.org/10.1016/j.marenvres.2020.105074.

Domínguez, R., Vázquez, E., Woodin, S.A., Wethey, D.S., Peteiro, L.G., Macho, G., Olabarria, C., 2020. Sublethal responses of four commercially important bivalves to low salinity. Ecol. Indic. 111, 106031.

Evans, G., Prego, R., 2003. Rias, estuaries and incised valleys: is a ria an estuary? Mar. Geol. 196, 171–175. https://doi.org/10.1016/S0025-3227(03)00048-3.

Fanjul, E.A., Gómez, B.P., Sánchez-Arévalo, I.R., 1997. A description of the tides in the Eastern North Atlantic. Prog. Oceanogr. 40, 217–244. https://doi.org/10.1016/S0079-6611(98)00003-2.

FAO (Ed.), 2016. Contributing to Food Security and Nutrition for all, the State of World Fisheries and Aquaculture Rome.

Feldman, A.D., 2000. Hydrologic Modeling System HEC-HMS: Technical Reference Manual. USA Army Corps of Engineers, Washington, DC, USA; Hydrologic Engineering Center: Davis, CA, USA.

Fernández-Nóvoa, D., García-Feal, O., González-Cao, J., de Gonzalo, C., Rodríguez-Suárez, J.A., Ruiz del Portal, C., Gómez-Gesteira, M., 2020. MIDAS: a new integrated flood early warning system for the Miño River. Water 12, 2319.

Filgueira, R., Guyondet, T., Comeau, L.A., Tremblay, R., 2016. Bivalve aquaculture-environment interactions in the context of climate change. Glob. Chang. Biol. 22, 3901–3913.

Fischer, E.M., Knutti, R., 2016. Observed heavy precipitation increase confirms theory and early models. Nat. Clim. Chang. 6, 986–991.

Fraga, I., Cea, L., Puertas, J., 2020. MERLIN: a flood hazard forecasting system for coastal river reaches. Nat. Hazards 100, 1171–1193.

Gledhill, J.H., Barnett, A.F., Slattery, M., Willett, K.L., Easson, G.L., Otts, S.S., Gochfeld, D.J., 2020. Mass mortality of the eastern oyster Crassostrea virginica in the Western Mississippi sound following unprecedented Mississippi River flooding in 2019. J. Shellfish Res. 39, 235–244.

Gomez-Gesteira, M., Moreira, C., Alvarez, I., deCastro, M., 2006. Ekman transport along the Galician coast (northwest Spain) calculated from forecasted winds. J. Geophys. Res. 111. https://doi.org/10.1029/2005JC003331.

González-Cao, J., García-Feal, O., Fernández-Nóvoa, D., Domínguez-Alonso, J.M., Gómez-Gesteira, M., 2019. Towards an automatic early warning system of flood hazards based on precipitation forecast: the case of the Miño River (NW Spain). Nat. Hazards Earth Syst. Sci. 19.

Gosling, E., 2008. Bivalve Molluscs: Biology, Ecology and Culture. John Wiley & Sons.

Hosseinzadehtalaei, P., Tabari, H., Willems, P., 2020. Climate change impact on short-duration extreme precipitation and intensity–duration–frequency curves over Europe. J. Hydrol. 590, 125249.

Iglesias, J., García-Gil, S., 2007. High-resolution mapping of shallow gas accumulations and gas seeps in San Simón Bay (Ría de Vigo, NW Spain). Some quantitative data. Geo-Mar. Lett. 27, 103–114.

Kharin, V.V., Zwiers, F.W., Zhang, X., Wehner, M., 2013. Changes in temperature and precipitation extremes in the CMIP5 ensemble. Clim. Chang. 119, 345–357.

Kotz, S., Nadarajah, S., 2000. Extreme Value Distributions: Theory and Applications. World Scientific.

Kunkel, K.E., Andsager, K., Easterling, D.R., 1999. Long-term trends in extreme precipitation events over the conterminous United States and Canada. J. Clim. 12, 2515–2527.

Lorenzo, M.N., Alvarez, I., 2020. Climate change patterns in precipitation over Spain using CORDEX projections for 2021–2050. Sci. Total Environ. 723, 138024.

Martínez-Conde, R.R., Puga-Rodríguez, J., Vila-García, R., Díaz-Fierros, F., Alvarez-Enjo, M., 2000. Las inundaciones recientes en Galicia. Ser. Geogr. 9, 187–210.

de Melo-Gonçalves, P., Rocha, A., Santos, J.A., 2016. Robust inferences on climate change patterns of precipitation extremes in the Iberian Peninsula. Phys. Chem. Earth Pt. A/B/C 94, 114–126.

Ministerio de Fomento, 2016. Norma 5.2-IC Drenaje superficial de la Instrucción de Carreteras. Spain Government, Madrid.

Mukherjee, S., Aadhar, S., Stone, D., Mishra, V., 2018. Increase in extreme precipitation events under anthropogenic warming in India. Weather Clim. Extr. 20, 45–53.

Munroe, D., Tabatabai, A., Burt, I., Bushek, D., Powell, E.N., Wilkin, J., 2013. Oyster mortality in Delaware Bay: impacts and recovery from hurricane Irene and tropical storm Lee. Estuar. Coast. Shelf Sci. 135, 209–219.

Myhre, G., Alterskjær, K., Stjern, C.W., Hodnebrog, Ø., Marelle, L., Samset, B.H., Sillmann, J., Schaller, N., Fischer, E., Schulz, M., 2019. Frequency of extreme precipitation increases extensively with event rareness under global warming. Sci. Rep. 9, 1–10.

Onen, F., Bagatur, T., 2017. Prediction of flood frequency factor for Gumbel distribution using regression and GEP model. Arab. J. Sci. Eng. 42 (9), 3895–3906.

Parada, J.M., Molares, J., 2008. Natural mortality of the cockle Cerastoderma edule (L.) from the Ria of Arousa (NW Spain) intertidal zone. Rev. Biol. Mar. Oceanogr. 43, 501–511.

Parada, J.M., Molares, J., Otero, X., 2012. Multispecies mortality patterns of commercial bivalves in relation to estuarine salinity fluctuation. Estuar. Coasts 35, 132–142.

Peteiro, L.G., Woodin, S.A., Wethey, D.S., Costas-Costas, D., Martínez-Casal, A., Olabarria, C., Vázquez, E., 2018. Responses to salinity stress in bivalves: evidence of ontogenetic changes in energetic physiology on Cerastoderma edule. Sci. Rep. 8, 1–9.

Pourmozaffar, S., Tamadoni Jahromi, S., Rameshi, H., Sadeghi, A., Bagheri, T., Behzadi, S., Gozari, M., Zahedi, M.R., Abrari Lazarjani, S., 2020. The role of salinity in physiological responses of bivalves. Rev. Aquac. 12, 1548–1566.

Scharffenberg, B., Bartles, M., Brauer, T., Fleming, M., Karlovits, G., 2018. Hydrologic Modeling System (HEC-HMS). User's Manual: Version 4.3. USA Army Corps of Engineers, Washington, DC, USA.

Sobral, P., Fernandes, S., 2004. Physiological responses and scope for growth of Ruditapes decussatus from Ria Formosa, southern Portugal, exposed to increased ambient ammonia. Sci. Mar. 68, 219–225.

Sousa, M.C., Vaz, N., Alvarez, I., Gomez-Gesteira, M., Dias, J.M., 2014. Influence of the Minho River plume on the Rias Baixas (NW of the Iberian Peninsula). J. Mar. Syst. 139, 248–260. https://doi.org/10.1016/j.jmarsys.2014.06.012.

Sousa, M.C., Ribeiro, A., Des, M., Gomez-Gesteira, M., DeCastro, M., Dias, J.M., 2020. NW Iberian Peninsula coastal upwelling future weakening: competition between wind intensification and surface heating. Sci. Total Environ. 703, 134808. https://doi.org/10.1016/j.scitotenv.2019.134808.

Stocker, T.F., Qin, D., Plattner, G.-K., Tignor, M.M., Allen, S.K., Boschung, J., Nauels, A., Xia, Y., Bex, V., Midgley, P.M., 2014. Climate Change 2013: The Physical Science Basis. Contribution of Working Group I to the Fifth Assessment Report of IPCC the Intergovernmental Panel on Climate Change. Cambridge University Press.

Taboada, J.J., Prego, R., Ruiz-Villarreal, M., Gómez-Gesteira, M., Montero, P., Santos, A.P., Pérez-Villar, V., 1998. Evaluation of the seasonal variations in the residual circulation in the Ría of Vigo (NW Spain) by means of a 3D Baroclinic model Taboada et al 1998.pdf. Estuar. Coast. Shelf Sci. 47, 661–670. https://doi.org/10.1006/ecss.1998.0385.

U.S. Army Corps of Engineers, 2018. Hydrologic Modeling System (HEC-HMS) User's 463 Manual: Version 4.3. Institute for Water Resources Davis: Hydrologic 464 Engineering Center.

Vázquez, M., Nieto, R., Liberato, M.L., Gimeno, L., 2020. Atmospheric moisture sources associated with extreme precipitation during the peak precipitation month. Weather Clim. Extr. 30, 100289.

Verdelhos, T., Marques, J.C., Anastácio, P., 2015. The impact of estuarine salinity changes on the bivalves Scrobicularia plana and Cerastoderma edule, illustrated by behavioral and mortality responses on a laboratory assay. Ecol. Indic. 52, 96–104.
Vilas, F., 2009. Rías and tidal-sea estuaries. Coastal Zones and Estuaries. 285.
Woodin, S.A., Wethey, D.S., Olabarria, C., Vazquez, E., Dominguez, R., Macho, G., Peteiro, L., 2020. Behavioral responses of three venerid bivalves to fluctuating salinity stress. J. Exp. Mar. Biol. Ecol. 522, 151256.
Yue, S., Ouarda, T.B., Bobée, B., Legendre, P., Bruneau, P., 1999. The Gumbel mixed model for flood frequency analysis. J. Hydrol. 226 (1–2), 88–100.